# INTERFACE WAVES IN A THIN SEDIMENT LAYER: REVIEW AND CONDITIONS FOR HIGH LOSS

M A Ainslie CORDA Ltd., Apex Tower, 7 High Street, New Malden, Surrey, KT3 4LH, England, UK

## 1. INTRODUCTION

Acoustic propagation in shallow water often results in repeated interaction with the sea bed, especially during the summer when surface heating can lead to strong downward refraction. As a result, forward and inverse acoustic modelling have been the subject of much research interest [1-6].

This article is concerned with reflection of plane waves from a sea bed comprising a sediment layer overlying a uniform half-space. Equations for the reflection coefficient are reviewed briefly in Section 2 for cases of varying complexity, first for a fluid sediment layer and then for a solid. This is followed by an analysis in Section 3 of the conditions necessary for high losses resulting from the generation of interface waves at the sediment-substrate boundary. A solid substrate is necessary for an interface wave to occur, but in Sec. 3 important additional effects due to *sediment* rigidity [3] are mostly ignored for simplicity.

## 2. REVIEW OF EQUATIONS FOR THE REFLECTION COEFFICIENT

### 2.1 Coherent Reflection Coefficient for a Fluid Sediment

The effect of layering in the seabed on the reflection coefficient has long been the subject of research interest [1-4]. Good agreement between theoretical predictions and propagation measurements is reported by Hughes et al [7] and by Tollefsen [8], demonstrating the need in general to model the sea bed as a layered solid medium. This Section reviews published equations for the reflection coefficient for scenarios of increasing complexity starting with the simple fluid model illustrated by Fig. 2.1.

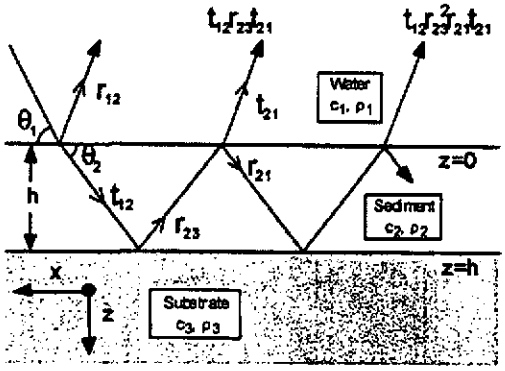


*Fig 2.1 – Ray paths for geometric series (fluid sediment)*

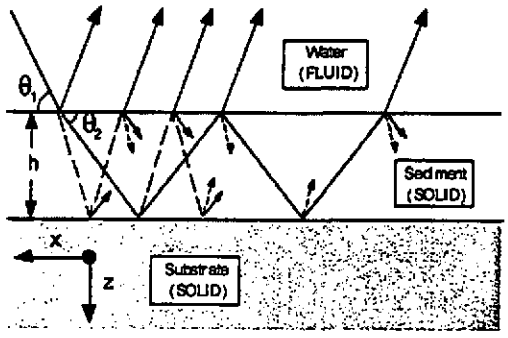


*Fig 2.2 – Proliferation of ray paths (solid sediment). The dashed lines indicate shear waves*

The reflection coefficient for this case is given by the geometric series [9]

$$r = r_{12} + t_{12} r_{23} t_{21} \sum_{n=0}^{\infty} (r_{23} r_{21})^n \tag{2.1}$$

$$= r_{12} + \frac{t_{12} r_{23} t_{21}}{1 - r_{23} r_{21}} \tag{2.2}$$

where $r_{ij}$ and $t_{ij}$ are the usual Rayleigh reflection and transmission coefficients defined in the obvious way, except that $r_{23}$ must include a two-way phase contribution so that (for example)

$$r_{12} = \frac{\zeta_{12} - 1}{\zeta_{12} + 1} \tag{2.3}$$

and

$$r_{23} = \frac{\zeta_{23} - 1}{\zeta_{23} + 1} e^{2i\gamma_2 h}, \tag{2.4}$$

where $\zeta_{ij}$ is the impedance ratio expressed in terms of the densities $\rho_i$ and vertical wave numbers $\gamma_i$

$$\zeta_{ij} = \frac{\rho_j \gamma_i}{\rho_i \gamma_j}. \tag{2.5}$$

The intuitive ray derivation of Eq. (2.2) makes it easily generalised to more complicated cases. For example it applies to a solid substrate provided that Eq. (2.4) is replaced with the appropriate fluid-solid reflection coefficient (see Sec. 3.2). If the sediment itself is layered this can be dealt with either by treating it as a continuously varying medium [10, 11] or by recursive application of Eq. (2.2) on a stack of uniform layers [9].

## 2.2 Incoherent Formula

Another advantage of Eq. (2.2) is that it can be averaged analytically over frequency to provide an incoherent formula useful for broadband applications [10]

$$R = R_{12} + \frac{T_{12} R_{23} T_{21}}{1 - R_{23} R_{21}} + \frac{2R_{23}}{1 - R_{23} R_{21}} \mathrm{Re}\left[t_{21}\left(r_{12} t_{12}^{*} + t_{12} r_{21}^{*}\right)\right] \tag{2.6}$$

where upper case symbols are used to indicate the power reflection and transmission coefficients

$$R_{ij} = |r_{ij}|^2 \tag{2.7}$$

and

$$T_{ij} = 1 - R_{ij}. \tag{2.8}$$

The first two terms of Eq. (2.6) are analogous to those of Eq. (2.2) and can be derived by incoherent addition of multipaths [10]. The third term is a systematic interference residual remaining after averaging over a full cycle. This term is usually small and reduces to zero at high frequency or for an isovelocity sediment.

## 2.3 Solid Sediment

For a solid sediment, the exponentiation of ray paths due to p-s and s-p mode conversion at each boundary means that keeping track of all rays appears to become an intractable problem (Fig. 2.2). Nevertheless Eq. (2.2) still applies in the following matrix form [12]

$$\mathbf{r} = \mathbf{r}_{12} + \mathbf{t}_{12}(\mathbf{1} - \mathbf{r}_{23}\mathbf{r}_{21})^{-1}\mathbf{r}_{23}\mathbf{t}_{21} \tag{2.9}$$

where

$$\mathbf{r}_{ij} = \begin{pmatrix} r_{ij}^{pp} & r_{ij}^{ps} \\ r_{ij}^{sp} & r_{ij}^{ss} \end{pmatrix} \tag{2.10}$$

and

$$\mathbf{t}_{ij} = \begin{pmatrix} t_{ij}^{pp} & t_{ij}^{ps} \\ t_{ij}^{sp} & t_{ij}^{ss} \end{pmatrix}. \tag{2.11}$$

The left hand side of Eq. (2.9) is a 2x2 matrix whose top left element is the reflection coefficient for a compressional wave. The other three elements involve either an incident or reflected shear wave and are of no interest here because the upper medium is a fluid (water).

A slight modification to the coefficients $r_{ij}^{\alpha\beta}$ and $t_{ij}^{\alpha\beta}$ allows for treatment of rough boundaries [13]. Equation (2.9) can also be applied to problems involving porous media although $\mathbf{r}_{ij}$ and $\mathbf{t}_{ij}$ then become 3x3 matrices to cater for the additional slow wave [14]. Even anisotropic media can be treated in the same way, albeit requiring a generalisation of the unit matrix to allow for different properties of upward and downward travelling waves [15].

## 2.4 Interface Waves

An interface wave or boundary wave [16] is a form of wave motion whose amplitude decays exponentially with distance away from the boundary between two media. A long way from the boundary the field decays effectively to zero and under these circumstances the interface wave, once generated, can exist in isolation – without the need for an incident field. The combination of zero incident field and non-zero total field leads to the paradoxical (though correct) conclusion that the reflection coefficient must be infinite [17]. There is no conflict with the principle of energy conservation because the evanescent wave carries no energy either towards or away from the boundary.

For example a plane wave travelling at the appropriate phase speed can excite a Stoneley wave at the lower boundary and this happens when the denominator of $r_{23}$ is zero (ie $\zeta_{23} \to -1$). A second kind of interface wave, associated with a resonant behaviour in the whole sediment layer (rather than with either of the two boundaries) arises in the limit $r_{23}r_{21} \to +1$, corresponding to a zero denominator in Eq. (2.2). The conditions required for both types are considered further in Section 3.

## 2.5 Finite Beams and Spherical Waves

The scope of this article is deliberately restricted to plane waves, and thus excludes important effects such as beam displacement [18] and caustics [10] which result from the reflection of finite beams and spherical waves. A comprehensive text on this subject is provided by Brekhovskikh and Godin [19].

# 3. EFFECT OF INTERFACE WAVES

## 3.1 Description of Sea Bed Layering

Consider a sea bed based on that of Fig. 2.1, comprising a fluid sediment layer of sound speed $c_2$ but overlying a *solid* substrate of compressional speed $c_p$ and shear speed $c_s$. The sediment is assumed to be sufficiently thin to neglect refraction within the layer. It is further assumed that $c_2$, $c_p$ and $c_s$ are all larger than $c_1$, the sound speed in water, so that the corresponding critical angles $\alpha_i$ are given by

$$\cos\alpha_i = c_1 / c_i \tag{3.1}$$

where i = 2, p or s. For a plane wave of angular frequency $\omega$ and grazing angle $\theta_1$ (in water) the vertical wave numbers are

$$\gamma_i = (\omega / c_i)\sin\theta_i \tag{3.2}$$

where the angles $\theta_i$ are related by Snell's law in the obvious way. Finally it is assumed that energy dissipation occurs either in the sediment or substrate, but not necessarily in both.

It is well known that under these conditions, and if the critical angles are sufficiently large, it is possible to excite high amplitude evanescent waves in the sediment resulting in high reflection losses when the acoustic wavelength is comparable with the sediment thickness h. These losses result from two types of behaviour: a Stoneley wave excited at relatively high frequencies, and an evanescent resonance excited at low frequency and near grazing incidence. The conditions giving rise to the high losses are investigated by Hovem and Kristensen [20]. Their analysis is extended in Sec. 3.2 below, clarifying the conditions required for high losses generally and the low frequency resonance in particular. Section 3.3 calculates the reflection loss vs angle at resonance and investigates how this function varies with the sediment critical angle $\alpha_2$.

## 3.2 Criterion for High Loss

### 3.2.1 Reflection Coefficient

For the problem in hand it is convenient to rearrange Eq. (2.2) for the reflection coefficient in the form [10]

$$r = \frac{r_{12} + r_{23}}{1 + r_{12} r_{23}} \tag{3.3}$$

where $r_{ij}$ are given by Eqs. (2.3) and (2.4). For the fluid-solid (i.e., sediment-substrate) boundary the impedance ratio becomes

$$\zeta_{23} = \frac{\rho_3 \gamma_2}{\rho_2}\left(\frac{\cos^2 2\theta_s}{\gamma_p} + \frac{\sin^2 2\theta_s}{\gamma_s}\right). \tag{3.4}$$

It is clear from Eq. (3.3) that a necessary condition for high loss is

$$|r_{12} + r_{23}| << 1. \tag{3.5}$$

The present interest is in grazing angles $\theta_1$ less than the smallest of the critical angles (denoted $\alpha_c$) so that all waves in the sediment and substrate are evanescent ones, with imaginary vertical wave numbers. Equation (3.5) can then be written

$$\frac{1+\zeta_{23}}{1-\zeta_{23}} \approx \frac{1}{r_{12}} e^{-2|\gamma_2|h}, \tag{3.6}$$

the left hand side of which is real (ignoring for now the small imaginary part of $\zeta_{23}$ due to attenuation). Equation (3.6) can therefore only be satisfied if the right hand side is either also real ($r_{12} \approx \pm 1$) or very small ($e^{-2|\gamma_2|h} << 1$). The $r_{12}=+1$ solution is associated with a non-evanescent resonance at infinite frequency and is not considered further. The other two options are examined below. Before this is done in detail an example from Hovem and Kristensen [20] is considered which includes features resulting from both cases of interest. Figure 3.1 shows reflection loss (−20 log|r|) versus frequency and angle for the parameters of Table I, with two different values for the sediment attenuation $\beta_2$. The Table I values are referred to as "HK" parameters and unless otherwise stated they are used in all subsequent graphs. The sediment thickness h is 10m. In the following it is shown that the high loss features marked S and E correspond respectively to a Stoneley wave (small $e^{-2|\gamma_2|h}$) and a resonant evanescent wave excited when $r_{12} \approx -1$, the frequency of which depends linearly on the sediment thickness and sound speed and logarithmically on the impedance ratio $\zeta_{23}$.

*Table I – Hovem-Kristensen (HK) sea bed model*

| Layer | density $\rho$(g/cm$^3$) | compressional speed (m/s) | compressional attenuation (dB/λ) | shear speed (m/s) | shear attenuation (dB/λ) |
|---|---|---|---|---|---|
| 1 (water) | 1.0 | 1500 | 0.0 | - | - |
| 2 (sediment) | 2.0 | 1700 | 0.8 | - | - |
| 3 (substrate) | 2.5 | 4700 | 0.3 | 2300 | 0.15 |

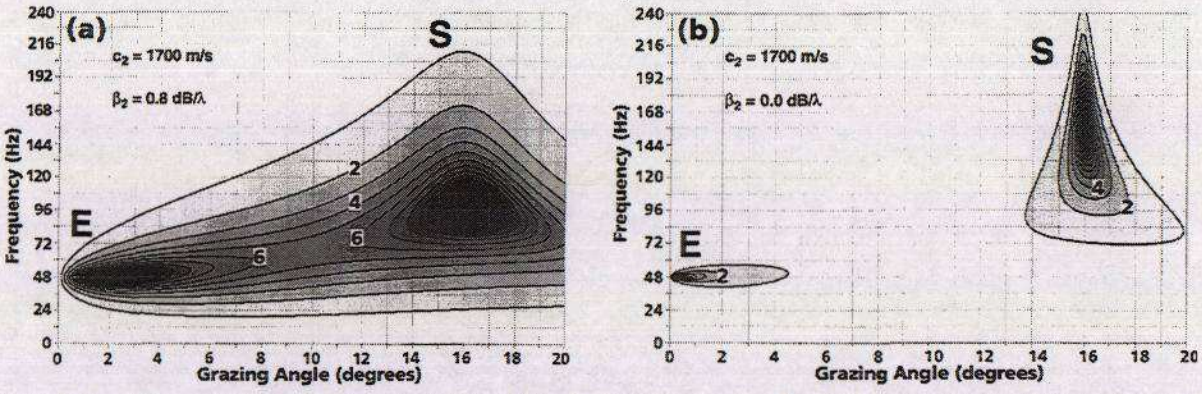


*Fig. 3.1 – Plane wave reflection loss vs angle $\theta_1$ and frequency for HK parameters with a) $\beta_2$=0.8 dB/λ, b) $\beta_2$=0. Contour levels are 1-10 dB in 1 dB steps*

### 3.2.2 Stoneley Wave

The high frequency case (large $|\gamma_2|h$) leads to the condition

$$1+\zeta_{23} \approx \frac{2}{r_{12}} e^{-2|\gamma_2|h} \tag{3.7}$$

Substituting for $\zeta_{23}$ using Eq. (3.4) and multiplying through by $(\rho_2\gamma_p/\rho_3\gamma_2)\sec^4\theta_s$ this becomes

$$\left(2-\frac{\sigma^2}{c_s^{\,2}}\right)^2+\frac{\rho_2\sigma^4}{\rho_3 c_s^{\,4}}\left(\frac{1-\sigma^2/c_p^{\,2}}{1-\sigma^2/c_2^{\,2}}\right)^{1/2}\left(1-\frac{2e^{-2|\gamma_2|h}}{r_{12}}\right)=4\left(1-\frac{\sigma^2}{c_p^{\,2}}\right)^{1/2}\left(1-\frac{\sigma^2}{c_s^{\,2}}\right)^{1/2} \qquad (3.8)$$

where $\sigma$ is the Snell invariant $c_i/\cos\theta_i$. At high frequency Eq. (3.8) reduces to the condition for a Stoneley–type interface wave of speed $\sigma$ at a fluid-solid boundary [16]. Substituting for the HK parameters in this limit gives $\sigma$=1560 m/s corresponding to an angle of 16°, and this shows up as feature S in Fig. 3.1. (Fig. 3.1b in particular).

Consider a frequency near the centre of feature S (100 Hz). Figure 3.2 shows the vector intensity (see Appendix A) plotted as a function of depth and incident grazing angle for this frequency. The Stoneley wave travels horizontally at the sediment-substrate boundary so a large tangential component at this depth is expected, as confirmed by Fig. 3.2a. By contrast the normal component has decayed almost to zero at the same depth (Fig. 3.2b). Notice also that the normal component varies continuously (and monotonically) with depth such that $dI_z/dz \leq 0$, as required by conservation of energy. The tangential component is discontinuous at both boundaries because of the step changes in density.

The field as a function of depth z in the sediment is given by Eq. (A.10) which for the high loss condition ( $r_{23} = -r_{12}$ ) becomes

$$\varphi(z)=\frac{\rho_1}{\rho_2}\frac{\exp(-|\gamma_2|z)-r_{12}\exp(+|\gamma_2|z)}{1-r_{12}} \qquad (3.9)$$

so at high frequency ($|\gamma_2|h \gg 1$) the field increases exponentially towards the lower boundary, the amplitude being limited (in this simple model) only by attenuation in the sediment or substrate; in the absence of attenuation such a wave is trapped at the lower boundary and, once generated, can exist without the need for an incident field. At any finite frequency though, even without attenuation some of this energy is re-radiated into the upper medium and the interface wave is a "leaky" one [17].

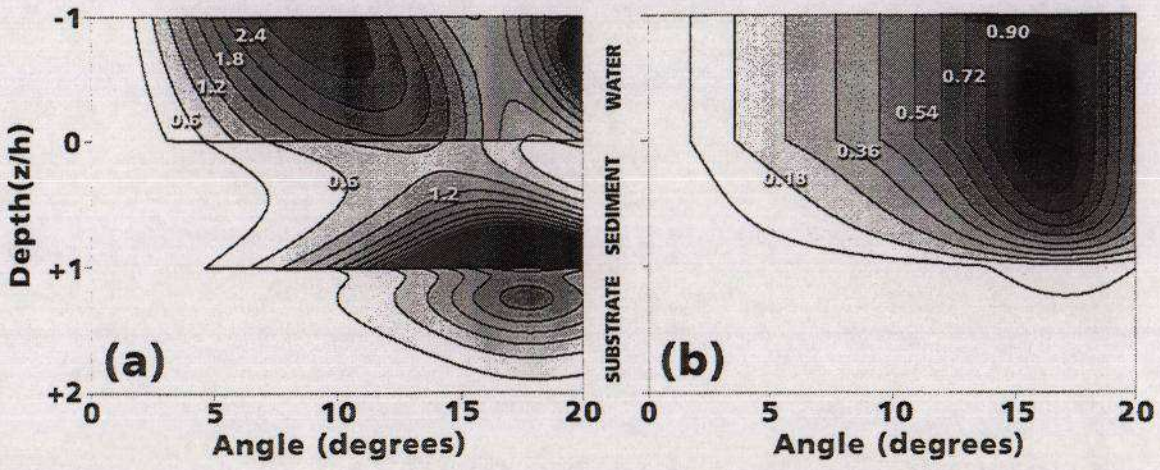


*Fig. 3.2 – Normalised vector intensity at 100Hz illustrating the effects due to the Stoneley wave: a) tangential component, normalised by dividing by the factor $-\omega^3\rho_1\kappa/2$; and b) normal component, normalised by $+\omega^3\rho_1\gamma_1/2$. Contour levels are a) 0.3 to 3.0 in steps of 0.3 and b) 0.09 to 0.9 in steps of 0.09.*

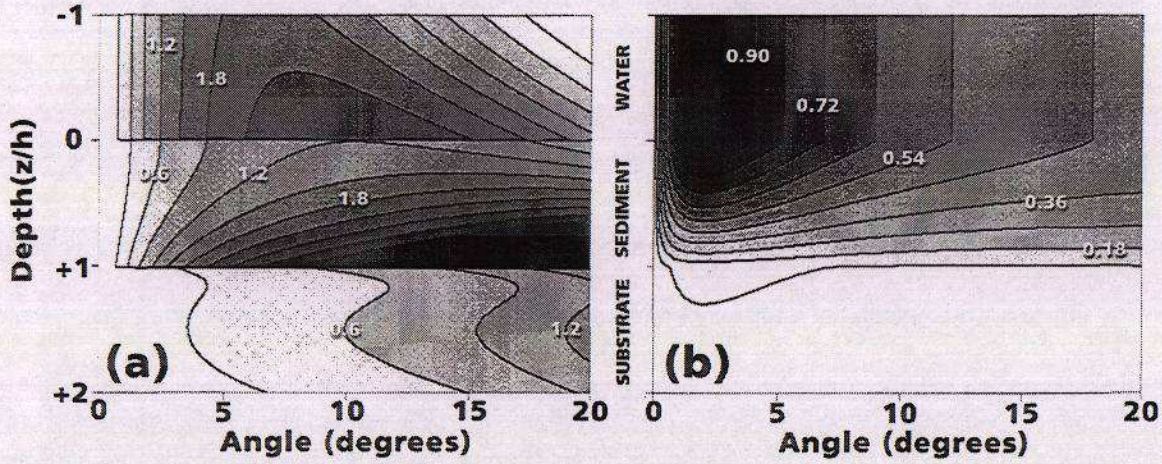


*Fig. 3.3 – Normalised vector intensity at 48 Hz illustrating effects due to the evanescent resonance: a) tangential and b) normal components. Contour levels are as Fig. 3.2.*

### 3.2.3 Evanescent Resonance

The alternative option ($r_{12} = -1$) implies a wave close to grazing incidence, for which Eq. (3.6) becomes

$$2\frac{\omega h}{c_2} = \cot\alpha_2 \ln\frac{\zeta_0 - 1}{\zeta_0 + 1} \tag{3.10}$$

where $\zeta_0$ is the impedance ratio $\zeta_{23}$ evaluated at $\theta_1$=0. For the HK parameters, Eq (3.10) gives a resonance frequency (denoted $f_E$) of 48Hz, in agreement with Fig. 3.1. At angles of interest here (up to about 5°) we see a gradual dissipation of the normal component as before (Fig. 3.3b), but no particular concentration of tangential energy as there was for the Stoneley wave (see Fig. 3.3a). Figure 3.1 (3.1b in particular) illustrates the narrowband nature of this effect, visible only in the immediate vicinity of the resonance frequency, contrasting with the broadband Stoneley wave which extends over an octave or so.

The field at resonance is again given by Eq. (3.9) but this time the frequency is prescribed by Eq. (3.10). Putting $r_{12} = -1$ in Eq. (3.9) and substituting for the resonance frequency we find

$$\varphi(z) = \frac{\rho_1}{\rho_2}\cosh\left[\frac{z}{2h}\ln\left(\frac{\zeta_0 - 1}{\zeta_0 + 1}\right)\right] \tag{3.11}$$

which is clearly bounded, with a maximum at z=h. With the exception of the limiting case $\zeta_0 \to -1$ (that is, an infinite resonance frequency), the field resulting from an evanescent resonance is always a leaky wave.

### 3.2.4 General Requirement

It is obvious by inspection of Eq. (3.10) that a real solution is possible if and only if

$$\zeta_0 < -1 \tag{3.12}$$

and this same inequality guarantees a solution to Eq. (3.7) at high frequency because for the assumed conditions ($c_p > c_s > c_1$ and $c_2 > c_1$) $\zeta_{23}$ increases from $\zeta_0$ at $\theta_1$=0 to a non-negative value at

$\theta_1=\alpha_c$. Assuming that this increase is monotonic it follows that inequality (3.12) is a necessary and sufficient condition for the existence of both features.

From Eq. (3.4) we find that

$$\zeta_0 = \frac{\rho_3 \sin\alpha_2}{\rho_2}\left[\text{cosec}\,\alpha_p - 4\tan^2\alpha_s \sec^2\alpha_s(\text{cosec}\,\alpha_s - \text{cosec}\,\alpha_p)\right]. \tag{3.13}$$

It follows that (3.12) can be expressed as a lower limit either on $\alpha_2$

$$(\rho_2/\rho_3)\text{cosec}\,\alpha_2 < 4\tan^2\alpha_s \sec^2\alpha_s(\text{cosec}\,\alpha_s - \text{cosec}\,\alpha_p) - \text{cosec}\,\alpha_p \tag{3.14}$$

or on $\alpha_p$

$$\text{cosec}\,\alpha_p < \frac{4\tan\alpha_s \sec^3\alpha_s - (\rho_2/\rho_3)\text{cosec}\,\alpha_2}{4\tan^2\alpha_s \sec^2\alpha_s + 1}. \tag{3.15}$$

Figures 3.4 and 3.5 illustrate these two inequalities in graphical form and can be used to predict whether a particular combination of parameters will result in high losses for a fluid sediment. Figure 3.4 shows threshold values of $(\rho_2/\rho_3)\text{cosec}\,\alpha_2$ as a function of $\cos\alpha_s$ and $\sqrt{2}\cos\alpha_p$. For a given combination of $c_p$ and $c_s$ we can read off a threshold (2.3 for HK as marked). High losses arise unless this threshold is exceeded. The actual HK value for the parameter $(\rho_2/\rho_3)\text{cosec}\,\alpha_2$ is 1.7, less than the threshold and consistent with observed high losses. Also of interest is the value of $\cos\alpha_S$ giving a *threshold* of 1.7 with $\cos\alpha_p$ fixed. The value (marked with a cross) is 0.72, corresponding to $c_s$=2080 m/s in agreement with the critical value quoted by Hovem and Kristensen [20]. Higher (lower) substrate shear speeds than this critical value result in high (low) losses for a fluid sediment as demonstrated by Fig. 5 of Ref. 20. Notice that the white region of our Fig. 3.4 indicates combinations of $\alpha_p$ and $\alpha_s$ for which high losses cannot arise for the mechanisms considered here. Increasing darkness levels indicate an increasing likelihood of high losses. The shaded region above the diagonal is forbidden on physical grounds, corresponding to a negative value of Poisson's ratio.

For the condition on $\alpha_p$ it is convenient to rewrite Eq. (3.15) as an upper limit on $\cos^2\alpha_p$ in the form

$$\frac{\cos^2\alpha_p}{\cos^2\alpha_s} < \frac{[4\tan\alpha_s \sec^3\alpha_s - (\rho_2/\rho_3)\text{cosec}\,\alpha_2]^2 - (4\tan^2\alpha_s \sec^2\alpha_s + 1)^2}{[4\tan\alpha_s \sec^2\alpha_s - (\rho_2/\rho_3)\cos\alpha_s \text{cosec}\,\alpha_2]^2}. \tag{3.16}$$

Figure 3.5 shows threshold values of $2\cos^2\alpha_p/\cos^2\alpha_s$ plotted as a function of $\cos\alpha_s$ and $\sqrt{(\rho_3/\rho_2)\sin\alpha_2}$. It is similar to Hovem and Kristensen's Fig. 7 except that here any combination of $\rho_3$, $\rho_2$ and $c_p$ is allowed (their Fig. 7 is restricted to $c_p/c_s$=2 and $\rho_3/\rho_2$=5/4), with the transition region between high and low losses shown explicitly.

Also apparent from Fig. 3.4 are *absolute* upper limits on $\cos\alpha_p$ and $\cos\alpha_s$ of 0.618 and 0.955 respectively (see Appendix B) for which high losses are possible due to interface waves. For a water sound speed value of 1500 m/s these limits translate to

$$c_p > 2430 \text{ m/s} \tag{3.17}$$

and

$$c_s > 1570 \text{ m/s}. \tag{3.18}$$

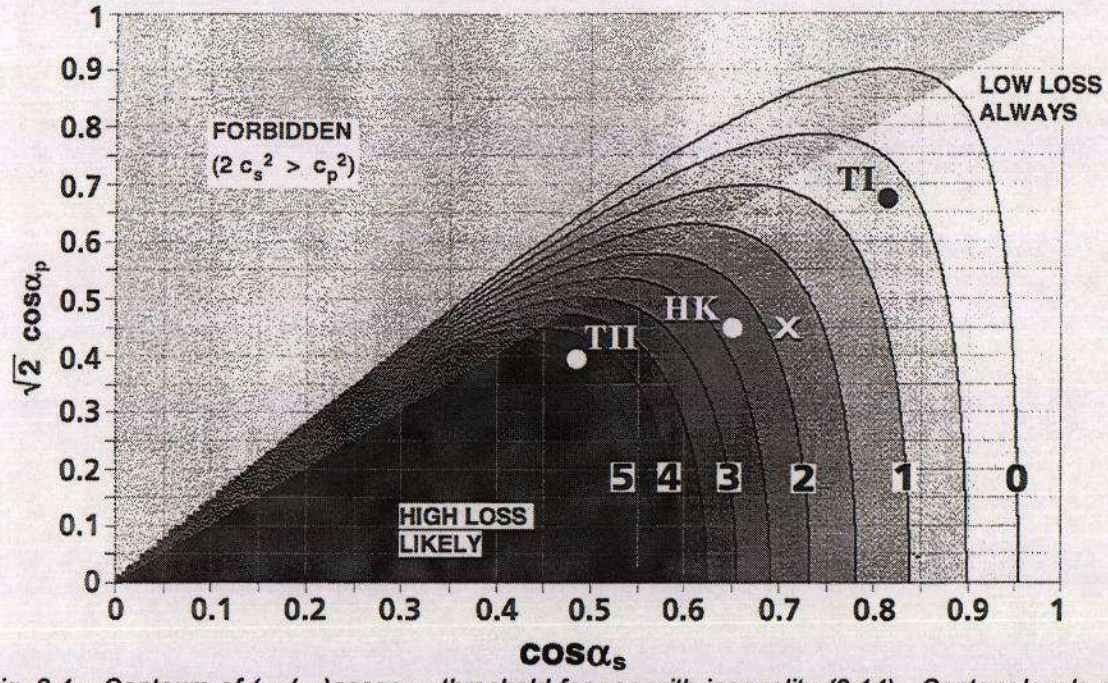


*Fig. 3.4 – Contours of $(\rho_2/\rho_3)\mathrm{cosec}\alpha_2$ threshold for use with inequality (3.14). Contour levels are 0 to 5 in steps of 0.5. The white region on the right marked "LOW LOSS ALWAYS" indicates conditions for which high losses cannot arise from the generation of interface waves, irrespective of sediment properties. The black region indicates that high losses are likely but not inevitable.*

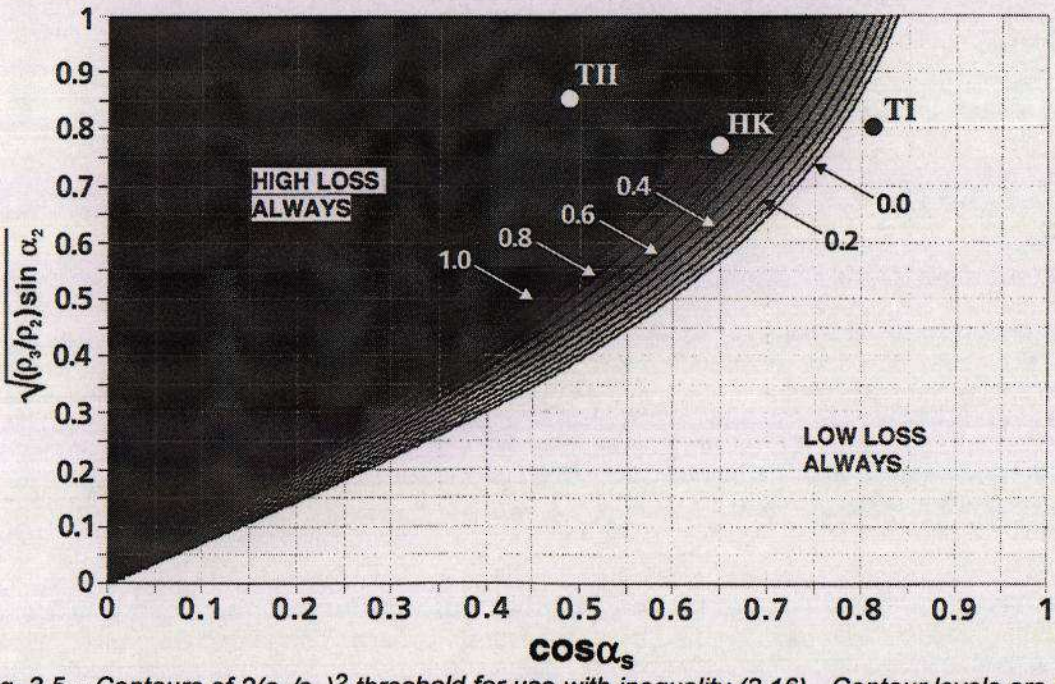


*Fig. 3.5 – Contours of $2(c_s/c_p)^2$ threshold for use with inequality (3.16). Contour levels are 0 to 1 in steps of 0.1. The white region on the right marked "LOW LOSS ALWAYS" indicates conditions for which high losses cannot arise from the generation of interface waves. Conversely, in the black region high losses are inevitable, irrespective of the substrate sound speed $c_p$.*

### 3.2.5 Critical Frequency

High losses due to interface waves are generated in a well defined range of frequencies, the lower limit of which is the evanescent resonance frequency $f_E$. The highest frequency that can satisfy Eq. (3.6) is determined by the imaginary part of $\zeta_{23}$, which depends in turn on the imaginary parts of $c_2$, $c_p$ and $c_s$. Assuming that the interface wave attenuation is dominated by absorption in the sediment, the impedance ratio evaluated at the Stoneley angle becomes

$$\zeta_{23} = -1 + \frac{i\delta_2}{|\sin^2\theta_2|} \tag{3.19}$$

where $\delta_2$ is the sediment absorption coefficient (in nepers per wave length). The upper frequency limit is then found by identifying the magnitude of the left and right sides of Eq. (3.6) which can only be equal at frequencies less than $f_S$ where

$$\frac{4\pi h}{c_2}|\sin\theta_2| f_S = \ln\frac{2|\sin^2\theta_2|}{\delta_2} \tag{3.20}$$

and $\theta_2$ is the (imaginary) sediment grazing angle satisfying the Stoneley condition:

$$|\sin\theta_2| = \left(c_2^{\,2}/\sigma^2 - 1\right)^{1/2}. \tag{3.21}$$

This critical frequency for the Stoneley wave $f_S$ is the highest frequency for which perfect cancellation can occur, and the interface wave amplitude is at its highest around this frequency, resulting in very high reflection losses. Above it the substrate interaction is reduced and losses become negligible at significantly higher frequencies. A practical upper limit is about $2f_S$.

Combining both limits results in the overall condition $f_E < f < 2\,f_S$, that is:

$$\cot\alpha_2 \ln\left(\frac{\zeta_0 - 1}{\zeta_0 + 1}\right) < \frac{4\pi h}{c_2} f < 2\left(\frac{c_2^{\,2}}{\sigma^2} - 1\right)^{-1/2} \ln\left[\frac{2(c_2^{\,2}/\sigma^2 - 1)}{\delta_2}\right]. \tag{3.22}$$

### 3.2.6 Examples

To test inequality (3.12) four examples (in addition to HK) of fluid sediment types with properties similar to those of Table I have been identified from recent publications [8,11]. The important properties of these sediments are summarised in Table II, showing the value of $\zeta_0$ and, where applicable, the evanescent resonance frequency $f_E$. Also included are the Stoneley wave speed $\sigma$ and critical frequency $f_S$ for each of the five sea beds. Notice that Tollefsen's Site I does not satisfy Eq. (3.12) and this explains the low losses observed for this case in his Fig. 1. In all other cases the criterion is satisfied and the predicted resonances are clearly visible at 15 Hz (Ainslie *et al* [11] Fig. 4b), 12 Hz (Tollefsen [8] Fig. 5a) and 125 Hz (Tollefsen [8] Fig. 6a). Tollefsen's sites I and II parameters are marked as TI and TII on Figs. 3.4 and 3.5. The remaining two parameter sets (columns 2 and 5 of Table II) are both close to HK.

The Ref. 11 results (column 2) are actually for a layered sediment with sound speed ratio increasing from 1.091 at the top to 1.194 at the bottom. The $c_2/c_1$ value quoted here is an effective sound speed ratio required to reproduce the same resonance frequency as the original profile, calculated from the equation

$$(c_2/c_1)_{\text{eff}} = [1 + (c_1\phi_0/\omega h)^2]^{-1/2} \tag{3.23}$$

where $\phi_0$ is calculated using Eq. (A18) of Ref. 11 for the phase difference between top and bottom of the sediment, and evaluated at grazing incidence. For an evanescent wave this "phase difference" is an imaginary number whose magnitude is the logarithmic decrement of the wave's amplitude.

*Table II – Summary of sea bed properties*

| | Hovem & Kristensen [20] and this paper (Table I) | Ainslie *et al* [11] (B2) | Tollefsen [8] (Site I) | Tollefsen [8] (Site II) | Tollefsen [8] (Site III) |
|---|---|---|---|---|---|
| $c_2/c_1$ | 1.133 | 1.151 | 1.088 | 1.088 | 1.172 |
| $c_p/c_1$ | 3.133 | 3.000 | 2.109 | 3.605 | 2.655 |
| $c_s/c_1$ | 1.533 | 1.600 | 1.224 | 2.091 | 1.552 |
| $\rho_3/\rho_2$ | 1.250 | 1.444 | 1.633 | 1.576 | 1.378 |
| $\zeta_0$ | −1.352 | −1.761 | −0.421 | −2.942 | −1.450 |
| h(m) | 10.0 | 20.0 | 20.0 | 18.0 | 3.0 |
| $c_1$ (m/s) | 1500.0 | 1500.0 | 1470.0 | 1470.0 | 1450.0 |
| $f_E$(Hz) | 48.2 | 15.5 | N/A | 11.7 | 124.9 |
| $\sigma$(m/s) | 1560 | 1613 | 1345 | 1579 | 1530 |
| $\delta_2$(Np/λ) | 0.0147 | 0.0091 | 0.0088 | 0.0185 | 0.0184 |
| $f_s$(Hz) | 101.3 | 62.3 | 44.9 | 46.0 | 301.6 |

### 3.2.7 Sediment Rigidity

The introduction of a small amount of sediment rigidity results in a train of shear waves generated at the lower boundary and travelling up through the sediment layer [21] and these can be modelled as described in Sec. 2.3. At low frequency these waves can contribute significantly to the reflected field and have been identified with a series of resonances at regular intervals in frequency [7, 22]. Interference between these additional multipaths and the evanescent compressional wave results in a shift in frequency of the evanescent resonance peak compared with Eq. (3.10) above. This point is illustrated by Tollefsen's Fig. 5 which shows the resonance frequency reduced from 12 Hz for a fluid sediment to 9 Hz for a solid.

## 3.3 Behaviour of Reflection Loss at Resonance

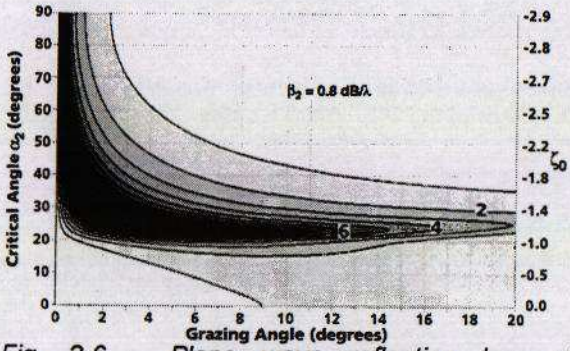


*Fig. 3.6 – Plane wave reflection loss at resonance vs grazing angle $\theta_1$ and critical angle $\alpha_2$. Contour levels are as Fig. 3.1*

Consider reflection loss vs angle evaluated at the resonance frequency $f_E$ for different values of $\zeta_0$, with particular attention to behaviour close to $\zeta_0$=−1. The value of $\zeta_0$ is controlled by varying $c_2$, keeping all other parameters fixed at their HK values. Figure 3.6 shows reflection loss vs angle $\theta_1$ and critical angle $\alpha_2$ at resonance. For large critical angles ($\alpha_2 > 40°, \zeta_0 < -1.8$) the expected peak can be seen near grazing incidence. For slightly smaller critical angles this peak broadens and at the same time moves to steeper angles; this effect reaches a maximum around $\alpha_2$=25°. For smaller critical angles still ($\alpha_2 < 20°, \zeta_0 > -1$) there is no resonance and the predicted losses are low; for illustrative purposes Fig. 3.6 uses a nominal resonance frequency of

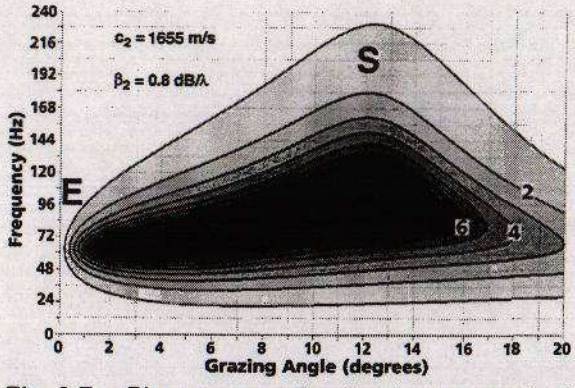


*Fig. 3.7 – Plane wave reflection loss vs angle $\theta_1$ and frequency ($c_2$=1655 m/s). Contour levels are as Fig. 3.1*

$$f_E = \left| \frac{c_1}{4\pi h \sin\alpha_2} \right| \mathrm{Re}\left[ \ln\left( \frac{\zeta_0 - 1}{\zeta_0 + 1} \right) \right] \qquad (3.24)$$

for all values of $\alpha_2$. A detailed examination of the behaviour near $\alpha_2$=25° ($c_2$ = 1655 m/s) shows that the value of $\zeta_{23}$ passes through –1 (the Stoneley wave condition) at $\theta_1$ = 12°. More significantly it stays close to –1 for all grazing angles up to about 20° and this explains the broad feature in Fig. 3.6. In other words the Stoneley wave and evanescent resonance coalesce into a single feature. This is demonstrated in Fig. 3.7 by plotting BL($\theta_1$,f) for $c_2$ = 1655 m/s. The nominal resonance frequency is 66 Hz but the influence of the broad band Stoneley wave results in high losses over a wide range of frequencies.

## 4. SUMMARY

Reflection of plane waves from a layered sea bed is considered. Simple equations for the reflection coefficient, in the form of a geometric series, are reviewed and shown to apply with surprising generality. The equations are used to derive a condition for high reflection loss resulting from the generation of interface waves in the sediment: the sediment and substrate critical angles must first be large enough to satisfy inequality (3.14); and second the acoustic wavelength must be of the same order as the sediment thickness such that inequality (3.22) is satisfied. It is shown that a necessary condition is for the substrate compressional and shear critical angles to exceed minimum values of 52° and 17° respectively, regardless of the sediment parameters.

## 5. ACKNOWLEDGEMENTS

The author thanks Dr A. J. Robins for numerous discussions, J. Kidwell for the artwork and S. Smithers for taming Microsoft Office.

## APPENDIX A - VECTOR INTENSITY CALCULATIONS

The purpose of this Appendix is to specify the calculations required for the intensity plots of Figs. 3.2 and 3.3. The derivation is for a solid medium and appropriate limiting cases are taken for the fluid sediment considered in the main text. Consider the time-averaged intensity vector $\underline{I}$ [23]

$$\underline{I} = -\frac{1}{2}\mathrm{Re}(\underline{v}^* \cdot \tau) \qquad (A.1)$$

where the particle velocity $\underline{v}$ and stress tensor $\tau$ are given as a function of the displacement $\underline{\varepsilon}$ and Lamé parameters ($\lambda$,$\mu$)

$$\underline{v} = \partial\underline{\varepsilon} / \partial t, \qquad (A.2)$$

$$\tau_{ij} = \lambda \delta_{ij} \underline{\nabla} \cdot \underline{\varepsilon} + \mu(\partial_i \varepsilon_j + \partial_j \varepsilon_i) \qquad (A.3)$$

$$\underline{\varepsilon} = \underline{\nabla}\varphi + \underline{\nabla} \wedge \underline{\psi} \qquad (A.4)$$

and $\varphi$,$\underline{\psi}$ are the usual potential functions. For the three-layer solid medium of Ref. 22, with a p wave incident from above we have

$$\varphi(x,z,t)e^{i(\kappa x+\omega t)} = \begin{cases} \exp(i\gamma_1^p z) + r^{pp}\exp(-i\gamma_1^p z) & (z \le 0) \\ \varphi_+ + \varphi_- & (0 < z \le h) \\ t^{pp}\exp[i\gamma_3^p (z-h)] & (z > h) \end{cases} \tag{A.5a}$$

$$\psi(x,z,t)e^{i(\kappa x+\omega t)} = \begin{cases} r^{ps}\exp(-i\gamma_1^s z) & (z \le 0) \\ \psi_+ + \psi_- & (0 < z \le h) \\ t^{ps}\exp[i\gamma_3^s (z-h)] & (z > h) \end{cases} \tag{A.5b}$$

where

$$\varphi_\pm = A_\pm^p \exp(\pm i\gamma_2^p z) \tag{A.6a}$$

$$\psi_\pm = A_\pm^s \exp(\pm i\gamma_2^s z) \tag{A.6b}$$

and the scalar $\psi$ is the y-component of the vector potential $\underline{\Psi}$; by symmetry the x and z components are zero. The reflection and transmission coefficients $r^{\alpha\beta}$, $t^{\alpha\beta}$ are derived in Ref. 22. Applying the same method for the amplitudes $A_{\pm}^{p,s}$ we obtain

$$A_+^p = d^{-1}\left[t_{12}^{pp}(1- < rr >^{ss}) + t_{12}^{ps} < rr >^{sp}\right] \tag{A.7a}$$

$$A_+^s = d^{-1}\left[t_{12}^{pp} < rr >^{ps} + t_{12}^{ps}(1- < rr >^{pp})\right] \tag{A.7b}$$

$$A_-^p = d^{-1}\left\{t_{12}^{pp}\left[(1- < rr >^{ss})r_{23}^{pp} + < rr >^{ps} r_{23}^{sp}\right] + t_{12}^{ps}\left[< rr >^{sp} r_{23}^{pp} + \left(1- < rr >^{pp}\right)r_{23}^{sp}\right]\right\} \tag{A.7c}$$

$$A_-^s = d^{-1}\left\{t_{12}^{pp}\left[(1- < rr >^{ss})r_{23}^{ps} + < rr >^{ps} r_{23}^{ss}\right] + t_{12}^{ps}\left[< rr >^{sp} r_{23}^{ps} + \left(1- < rr >^{pp}\right)r_{23}^{ss}\right]\right\} \tag{A.7d}$$

where

$$d = [(1- < rr >^{pp})(1- < rr >^{ss}) - < rr >^{ps} < rr >^{sp}] \tag{A.8}$$

and

$$< rr >^{\alpha\beta} = r_{23}^{\alpha p} r_{21}^{p\beta} + r_{23}^{\alpha s} r_{21}^{s\beta}. \tag{A.9}$$

In the main text the water and sediment layers are both fluids, so that $r^{ps}$, $\psi_+$ and $\psi_-$ are all zero. In this limit the sediment field simplifies, dropping superfluous superscripts, to

$$\varphi(z) = \frac{t_{12}}{1 + r_{12}r_{23}}\left[\exp(i\gamma_2 z) + r_{23}\exp(-i\gamma_2 z)\right] \qquad (0 < z \le h). \tag{A.10}$$

# APPENDIX B - CONDITIONS ON SUBSTRATE CRITICAL ANGLES

In the main text it is shown that high losses can only occur when the substrate critical angles $\alpha_p$ and $\alpha_s$ exceed certain minimum values regardless of the sediment sound speed. The purpose of this Appendix is to derive these minimum values.

## B.1 Shear Critical Angle $\alpha_s$

The lower limit on $\alpha_s$ is determined from Fig. 3.4 by the intersection of the x-axis ($\cos\alpha_p = 0$) with the zero contour, i.e.

$$\operatorname{cosec}\alpha_p + 4\tan^2\alpha_s \sec^2\alpha_s(\operatorname{cosec}\alpha_p - \operatorname{cosec}\alpha_s) = 0\,. \tag{B.1}$$

The result is a cubic equation in $\sin\alpha_s$

$$\sin^3\alpha_s + \sin^2\alpha_s + 3\sin\alpha_s - 1 = 0 \tag{B.2}$$

the solution of which is [24]

$$\sin\alpha_s = \frac{\sqrt{8}}{3}\left(A^{1/3} - A^{-1/3}\right) - \tfrac{1}{3} \tag{B.3}$$

$$A = \frac{13 + \sqrt{297}}{8\sqrt{2}}\,. \tag{B.4}$$

The lower limit on $\alpha_s$ for high losses is therefore

$$\cos\alpha_s < 0.9553 \qquad (\alpha_s > 17.2^\circ). \tag{B.5}$$

## B.2 Compressional Critical Angle $\alpha_p$

The lower limit on $\alpha_p$ is determined by the intersection of Eq. (B.1) with the diagonal $\cos\alpha_s = \sqrt{2}\cos\alpha_p$, from which we obtain a quadratic in $\cos^2\alpha_p$

$$\cos^4\alpha_p - 3\cos^2\alpha_p + 1 = 0\,. \tag{B.6}$$

The solution for $\cos\alpha_p$ is the golden ratio $(\sqrt{5}-1)/2$ so that the lower limit on $\alpha_p$ is

$$\cos\alpha_p < 0.6180 \qquad (\alpha_p > 51.8^\circ). \tag{B.7}$$

## REFERENCES

1. N. G. Pace (ed), *Acoustics and the Sea-Bed* (Bath University Press, Bath, 1983).
2. A. Lara Sáenz, C. Ranz Guerra & C. Carbó Fité (eds), *Acoustics and Ocean Bottom* (Consejo Superior de Investigaciones Científicas, Madrid, 1987).
3. J. M. Hovem, M. D. Richardson & R. D. Stoll (eds), *Shear Waves in Marine Sediments* (Kluwer, Dordrecht, 1991).
4. N. G. Pace & D. N. Langhorne (eds), Acoustic Classification and Mapping of the Seabed (Institute of Acoustics, St Albans, 1993).
5. O. Diachok, A. Caiti, P. Gerstoft & H. Schmidt (eds) *Full Field Inversion Methods in Ocean Seismo-Acoustics* (Kluwer, Dordrecht, 1995).
6. N. R. Chapman & A. Tolstoy, (eds) *Benchmarking Geoacoustic Inversion Methods,* Special issue of J. Comp. Acoust. Vol 6, March & June 1998.
7. S. J. Hughes, D. D. Ellis, D. M. F. Chapman & P. R. Staal, Low-frequency acoustic propagation loss in shallow water over hard-rock seabeds covered by a thin layer of elastic-solid sediment, J. Acoust. Soc. Am **88**, 283-297 (1990).
8. D. Tollefsen, Thin-sediment shear-induced effects on low-frequency broadband acoustic propagation in a shallow continental sea, J. Acoust. Soc. Am **104**, 2718-2726 (1998).
9. C. S. Clay & H. Medwin, *Acoustical Oceanography* (Wiley, New York, 1977).
10. M. A. Ainslie, Reflection and transmission coefficients for a layered fluid sediment overlying a uniform solid substrate, J. Acoust. Soc. Am **99**, 893-902 (1996).
11. M. A. Ainslie, A. J. Robins & M. K. Prior, Benchmark solutions of plane wave bottom reflection loss, J. Acoust. Soc. Am **104**, 3305-3312 (1998).
12. M. A. Ainslie, Comments on "Ultrasonic interferences in polymer plates" [J. Acoust. Soc. Am. **104**, 1232-1241], J. Acoust. Soc. Am, In press (1999).
13. O. I. Lobkis & D. E. Chimenti, Elastic guided waves in plates with surface roughness. I. Model calculation, J. Acoust. Soc. Am. **102**, 143-149 (1997).
14. G. S. Sammelmann, Biot-Stoll model of the high-frequency reflection coefficient of sea ice, J. Acoust. Soc. Am. **94**, 371-385 (1993).
15. S .I. Rokhlin & W. Huang, Ultrasonic wave interaction with a thin anisotropic layer between two anisotropic solids: Exact and asymptotic-boundary-condition methods, J. Acoust. Soc. Am. **92**, 1729-1742 (1992).
16. I. Tolstoy, Boundary Waves, *Encyclopaedia of Acoustics*, edited by M. J. Crocker (Wiley-Interscience, New York, 1997), pp153-159.
17. L. M. Brekhovskikh & O. A. Godin, *Acoustics of Layered Media I: Plane and Quasi-Plane Waves* (Springer, Berlin, 1990).
18. D. E. Weston, Wave shifts, beamshifts, and their role in modal and adiabatic propagation, J. Acoust. Soc. Am. **96**, 406-416 (1994).
19. L. M. Brekhovskikh & O. A. Godin, *Acoustics of layered Media II: Point Sources and Bounded Beams* (Springer, Berlin, 1992).
20. J. M. Hovem & A. Kristensen, Reflection loss at a bottom with a fluid sediment layer over a hard solid half-space, J. Acoust. Soc. Am **92**, 335-340 (1992).
21. P. J. Vidmar, Ray path analysis of sediment shear wave effects on bottom reflection loss, J. Acoust. Soc. Am **68**, 639-648 (1980).
22. M. A. Ainslie, Plane-wave reflection and transmission coefficients for a three-layered elastic medium, J. Acoust. Soc. Am **97**, 954-961 (1995); erratum [J. Acoust. Soc. Am **105**, 2053 (1999)]
23. B. A. Auld, *Acoustic Fields and Waves in Solids* (Wiley, New York, 1973), Vol. 1.
24. J. W. Archbold, *Algebra* (Pitman Publishing, London, 1970).